Submitted to Combustion Science and Technology, October 2007

LES Modelling of Premixed Deflagrating Flames in a Small Scale Vented Explosion Chamber with a Series of Solid Obstructions

S.R. Gubba
Wolfson school of Mechanical and Manufacturing Engineering
Loughborough University, Loughborough, LE11 3TU, UK

S.S. Ibrahim *
Aeronautical and Automotive Engineering
Loughborough University, Loughborough, LE11 3TU, UK

W. Malalasekera
Wolfson school of Mechanical and Manufacturing Engineering
Loughborough University, Loughborough, LE11 3TU, UK

A.R. Masri
School of Aerospace, Mechanical and Mechatronic Engineering
The University of Sydney, Sydney, NSW 2006, Australia

*Corresponding author: S.S.Ibrahim@lboro.ac.uk

Abstract: In this study, simulations of propagating turbulent premixed deflagrating flames past built in solid obstructions in a laboratory scale explosion chamber has been carried out with the Large Eddy Simulation (LES) technique. The design of the chamber allows for up to three baffle plates to be positioned in the path of the propagating flame, rendering different configurations, hence generating turbulence and modifying the structure of the reaction zone. Five important configurations are studied to understand the feedback mechanism between the flame-flow interactions and the burning rate. In LES, the sub-grid scale (SGS) reaction rate should be accounted for by an appropriate model which can essentially capture the physics. The present work has been carried by using the flame surface density (FSD) model for sub-grid scale reaction rate. The influence of the flow on turbulence and flame

propagation as a result of the in-built solid obstructions is also examined. The impact of the number and the position of such baffle plates on the generated overpressure, flame speed and structure are studied. Results from the simulations are compared with experimental data for five configurations and they show good agreement.

Key Words: LES modelling, Explosion, Deflagrating flames.

1 Introduction

Modelling of turbulent premixed explosions involved in deflagrating flames inside a confined chamber remains a challenging problem particularly with respect to the adequate representation of the burning rate and the structure of the reaction zone. The deflagrating flames may make a transition into detonation depending on boundary conditions, length and width of the chamber and the generated overpressure. Several experimental and numerical studies have been performed to evaluate the effect of the width and length of the chamber, with or without obstacles on accelerating flames (Williams (1985a), Aldredge et al. (1998), Bradley (2002), Lee & Lee (2003), Akkerman et al. (2006) and Bauwens et al. (2007)). Modelling of deflagrating flames is also of significant practical importance in engineering applications, such as spark ignitions engines, gas turbines, and industrial burners as well as in loss prevention analysis, in the case of accidental gas explosions. In all of these applications, the flame front interacts with complex solid boundaries and with the solid obstructions if present. These flames generate turbulence in the medium of propagation by vortex shedding and creating local wake/recirculation whereby the flame is wrapped in on

itself, increasing the surface area available for combustion and the rate of local reaction rate.

A large number of experimental studies were aimed at understanding the flame-turbulence interactions in vented explosion chambers with in-built solid obstructions (Moen et al. (1980), Hjertager et al. (1988), Starke and Roth (1989), Fairweather et al. (1996), Masri et al. (2000) and Bradley et al. (2001)). The generated turbulence was found to elongate the deflagrating flame front, hence extending the flame surface area, increasing the flame burning velocity and enhancing the flow velocity. In real explosions, acceleration of the flame front results from a complex interaction between the moving flame and the local blockage caused by the presence of equipments. Such blockage leads to a local acceleration of the flame front in the form of jetting which in turn forms a complex feedback system and may lead to unlimited flame acceleration. Such distortion in the flow field may also change the structure of the reaction zone leading to broadening and/or to local quenching depending on the local strain rates. Experimental and numerical studies have been partially successful in understanding such a complex feedback mechanism, which is vital for the smart control of the turbulent deflagrating flames.

Explosion chambers used by Moen et al. (1980 and 1982), Hjertager et al. (1988) and Bradly et al. (2001) to study the flame interaction issues yielded limited data because they involved large-scale experiments that did not lend themselves easily to detailed measurements. Starke and Roth (1989), Phylaktou and Andrews (1991), Fairweather et al. (1996), Lindstedt and Sakthitharan (1998), Masri et al. (2000) and Ibrahim et al. (2001b) have used laboratory scale chambers utilising simple geometrical

configurations that were adaptable to complex diagnostics and the subsequent validation of numerical models. All these studies have involved the use of a variety of obstacles (square/circle/triangular/wall baffles) in the path of propagating flames. However the exact mechanism that correlates flame structure, speed and resulting over pressure are not well understood yet. Masri et al. (2000) reported the influence of the size and shape of the solid obstacles and found that both the blockage ratio, as well as the shape of obstacles influences the flame structure and propagation rate. Lindstedt and Sakthitharan (1998) and Fairweather et al. (1999) reported the interaction of flames with baffle type obstacles with a high quality flame shape information as well as mean and fluctuating velocity data. The original experimental chamber of Masri et al. (2000 & 2006) and Ibrahim et al. (2001a) had a 20 litre volume and was found to be impractical for modelling studies due to the long LES computational times. An alternative design that preserved the same physics and optical access, yet with a reduced volume of less than a litre is now adopted (Kent et al., 2005).

Parallel to the experiments, there is a pressing need for an enhancement in the modelling capabilities of turbulent premixed combustion. Several studies in turbulent premixed flames in a variety of confined and semi-confined chambers (Patel et al. (2002), Pitsch & Lageneste (2002), Kirkpatrik et al. (2003), Fureby (2005) and Masri et al. (2006)) have been reported to date using Reynolds averaged Navier-Stokes (RANS) and large eddy simulations (LES) approaches. While direct numerical simulations (DNS), remain very expensive and not viable for high Reynolds number flows. Hence, LES has emerged as a powerful and effective diagnostic tool for handling large-scale turbulent motions, as the method is based on time resolved three

dimensional unsteady large scale turbulent motions. In LES, large scales are resolved with adequate spatial and temporal resolution, and small scales are modelled due to their isotropic nature, and contain less turbulent kinetic energy. LES has been successfully applied to a variety of reacting cases ranging from simple to complex flows, involved in fundamental and advanced studies such as aircraft engine combustion (Kim et al., 1999), combustion instabilities (Menon and Jou, 1991 and Fureby, 2000), small pool fires (Kang and Wen, 2004), swirling flames (Malalasekera et al., 2007) and large scale explosions (Molkov et al., 2004 and Makrov et al., 2007). In spite of the numerical and computational advancements, the crucial issue to the advancement of LES lies in the development of adequate sub-grid scale models that are capable of representing combustion over a wide range of conditions. This remains a key challenge facing the turbulent combustion community.

In the numerical modelling of turbulent premixed deflagrating flames, reaction rate is the most significant parameter to be computed and can be quantified by several approaches, such as flame surface density technique (Bray (1990) and Prasad and Gore (1999)) and flame tracking technique (Williams, 1985b) following the laminar flamelet concepts. Alternatively reaction rate can be estimated by following the artificial flame thickening approach (Veynante and Poinsot, 1997) and probability density function (PDF) approach (Möller et al., 1996). Recently Duwig and Fuchs (2007) simulated turbulent premixed flames by using S^+ marker field. They developed a new equation for marker field and it is expected to capture the laminar or turbulent flame propagation via a reactive diffusive balance.

With the flame surface density approach, either a full transport equation is solved for flame surface density Σ (Hawkes and Cant, 2001) or using an algebraic model (Boger et al., 1998) as a function of a reaction progress variable following the laminar flamelet assumption. The preliminary studies by Gubba et al. (2007) support the application of the dynamic flame surface density (DFSD) model (Knikker and Veynante, 2004), to simulate turbulent propagating flames in small scale chambers and identified the areas for the further development.

In flame tracking technique, assuming the flame is thin and it can be tracked by defining a scalar field *G*, the reaction rate is calculated as a function of turbulent burning velocity u_T which is a function of turbulence intensity and laminar burning velocity. The flame thickening approach involves in imposing a flame thickening factor by keeping laminar flame speed constant and allows resolving the flame front (reaction zone) on LES grid. This approach assumes, implicitly that chemistry rather than diffusive processes controls the reaction rate and hence the use of detailed chemical kinetics is recommended for better accuracy (Poinsot et al., 1991). This is numerically unattractive compared to the laminar flamelet approach where the chemistry is assumed to be fast and the reaction is largely controlled by transport processes. The use of probability density function (PDF) approaches to model combustion at the sub-grid level with LES for premixed combustion was first used by Möller et al. (1996). This approach is computationally expensive but is gradually receiving considerable attention as a potentially successful tool in premixed combustion. Linear eddy modelling (LEM) (McMurthy et al., 1993) which involves using a grid within a grid technique to solve the governing equations up to the required resolution is another useful sub-grid modelling approach for LES.

In the present study, the flame surface density approach is adopted where the chemistry is assumed to be fast and the filtered reaction rate is modelled by an algebraic relation of Boger et al. (1998) deduced from the DNS analysis. Following the recommendations made by Masri et al. (2000), Kent et al. (2005) designed the latest explosion chamber of 0.625 litres, allowing for use of repeated obstacles and to generate high levels of turbulence without the risk of deflagration to detonation transition. The novel feature of this chamber lies in the flexibility of using several configurations of premixed flame propagation based on the number and the position of the array of baffle plates (ABP) from the ignition end. This chamber also enables broad range of optical access and hence facilitates the use of laser-based diagnostic techniques. The small size of the chamber minimizes computational time required for LES and facilitates detailed analysis. Primarily five configurations with a different number and position of baffles plates are simulated here. Stagnant propane/air mixture having an equivalence ratio of 1.0 is used in the chamber and efforts have been made to identify the link between the resulting peak pressure and the amount of fuel/air mixture trapped behind the obstruction.

This paper is organized as follows: Section 2 describes the explosion chamber, importance of the individual baffle plates and their effect on the turbulence generation during the flame propagation. Section 3 delineates the governing equations and the LES model used in the present simulations. Section 4 presents the numerical procedures used in the LES calculations. Demonstration of the LES predictions and their comparisons with experimental measurements are presented and discussed in Section 5. The conclusions of the present investigation are summarized in Section 6.

2 The explosion chamber

As briefed in the introduction, the explosion chamber used here is the latest and third modification from the Sydney University group (Kent et al., 2005) and can accommodate series of baffle plates. It has a volume of 0.625 L with a square cross section of 50 mm and a length of 250 mm as shown in Figure 1. Experimental data for the flame structure and generated over-pressure have recently been published by Kent et al. (2005) and are used here for model validation. A maximum of three baffle plates can be positioned in the chamber at different downstream locations from the bottom ignition end. This chamber is of particular interest because of its smaller volume and potential to hold a flame propagating in strong turbulence. Another important feature of this chamber is the ability to rearrange the baffle plates into several configurations based on the number and the position of the baffle plates from the bottom of the ignition end. Figure 2 shows five individual configurations used in the present study. Configuration 1 has three baffles, configuration 2, 3 and 4 have two baffles each positioned at different locations and configuration 5 has just one baffle plate. One could consider the configurations without any obstructions and with only one solid square obstruction before studying the aforementioned configurations. However, from experimental studies of Kent et al. (2005) and a combined experimental and LES study by Masri et al. (2006), we have learned the influence of the individual baffles plates on turbulence and over pressure generation. Hence, the basic configurations are not considered here for LES simulations, in order to save the computational time.

The baffle plates used are of 50 x 50 mm aluminium frames constructed from 3 mm thick sheet. This consists of five 4 mm wide bars each with a 5 mm wide space

separating them, rendering a blockage ratio of 40%. The baffle plates are aligned at 90 degrees to the solid obstacle in the configuration employed in the present study. These baffle plates are named as S1, S2 and S3 and located at 20, 50 and 80 mm respectively from the ignition point. All the above configurations have a solid square obstacle of 12 mm in cross section which is centrally located at 96 mm from the ignition point running through out the chamber cross section, which causes significant disruption to the flow. The pressure is measured using Piezo-resistive pressure transducers with a range of 0-1bar and a response time of 0.1ms. The transducer utilizes quartz crystals to develop a charge relative to the pressure applied. The pressure transducer is positioned at the ignition end of the vessel. The exact location is on the central plane of x-axis, 37 and 5 mm on y and z axis respectively from the left bottom of the chamber.

2.1 Arrangement of baffle plates and solid obstacle

The introduction of baffle plates and the obstacle into the flow inside the chamber serve to increase the turbulence level and the flame propagation speed. The position and number of the baffle plates employed with respect to the square obstacle significantly alters the generated peak pressure, flame speed and structure (Kent et al., 2005). From the experimental investigations of Kent et al. (2005) it is found that the addition of baffle plates increases the overpressure, speeds up the flame and causes significant level of stretching in the flame front as it jets through the baffles. Higher turbulence levels increase the burning rates and achieve overpressures at an even faster rate than the flame speed. Hence large increase in overpressure can be gained through only a small increase in flame speed. In the present work, the influence of individual baffle plates and square obstacle on the flow is discussed with particular

relevance on how the solid obstructions placed inside the chamber change the turbulence level and the regime of combustion.

2.1.1 Baffle Plate One (S1) This plate is located at 20mm downstream from the ignition end. Due to its close proximity to the ignition point the flame speed is relatively low, thus this plate only has a small effect on turbulence generation. Hence re-laminarisation of the flame front occurs shortly after the flame crosses this baffle plate.

2.1.2 Baffle Plate Two (S2) This plate is located at 50mm downstream from the ignition closed end and serves both to increase the pressure and increase the propagation speed of the flame. In particular it affects the positioning of the flame front at peak overpressure.

2.1.3 Baffle Plate Three (S3) This plate is located at 80mm downstream from the ignition closed end and is most effective at increasing the amount of turbulence generated within the combustion chamber. This baffle accelerates the flame to about 50 m/s, thus increasing the amount of turbulence that can be generated by the obstruction.

2.1.4 Square Obstacle (Sq. Ob.) The solid square obstacle is located at 96 mm downstream from the ignition close end. This is not a turbulence-inducing device as such but does serve to increase the blockage ratio and hence alter the development of the flame front. Rapid acceleration of the flame is recorded past this obstruction followed by the wrapping of the flame in the recirculation region, which enhances the mixing and distortion at the flame front.

3 The LES models

To perform LES calculation of deflagrating flames inside vented explosion chamber, conservation equations of mass, momentum, energy and a reaction progress variable coupled with the state equation are required to solve. A low pass spatial filter (*F*) is implicitly applied to any flow variable $\phi(x,t)$ in the governing equations to separate large eddies from flow motions, such as:

$$\overline{\phi}(x,t) = \int_V F(x-x')\phi(x',t)dx' \tag{1}$$

Top-hat filter is applied to the governing equations in the present study as it naturally fits in to finite volume discretization. The integration is carried out over the entire flow domain *V*. The major challenges in LES to be accomplished are sub-grid-scale modelling of scalar fluxes and the chemical reaction. The standard Smagorinsky (1963) model is widely used to model the sub-grid fluctuations in the velocity field. The sub-grid scale contributions of turbulence to the momentum flux $\tau_{ij} = \overline{\rho}\left(\tilde{u}_i\tilde{u}_j - \widetilde{u_i u_j}\right)$ are computed as:

$$\tau_{ij} - \frac{1}{3}\delta_{ij}\tau_{kk} = -2\overline{\mu}_{\mathrm{SGS}}\left(\tilde{S}_{ij} - \frac{1}{3}\delta_{ij}\tilde{S}_{kk}\right) \tag{2}$$

where S_{ij} is the stress tensor, δ_{ij} is the Kronoker delta and μ_{SGS} is the eddy viscosity modelled as a function of the filter size and the strain rate,

$$\mu_{\mathrm{SGS}} = \overline{\rho}\left(C_s\overline{\Delta}\right)^2\left|\tilde{S}\right| \tag{3}$$

where $\left|\tilde{S}\right| = \sqrt{2\tilde{S}_{ij}\tilde{S}_{ij}}$ and C_s is a dimensionless Smagorinsky coefficient. Germano et al. (1991) extended this model by devising an automated procedure for determining

the Smagorinsky model coefficient. In the present simulations, model coefficient C_s is calculated from the instantaneous flow conditions using the dynamic determination procedure developed by Moin et al. (1991) for compressible flows.

Chemical reaction is modelled assuming a single step irreversible reaction between reactants and products. To avoid the Zeldovich instability (thermal diffusion), unit Lewis number i.e., Le = Pr/Sc =1 is considered. The reaction progress variable c defines the chemical status of mixture in the domain from unburned (c = 0) to burned (c = 1). Favre-filtered reaction progress variable equation can be written as:

$$\frac{\partial \bar{\rho}\tilde{c}}{\partial t} + \frac{\partial \left(\bar{\rho}\tilde{u}_j\tilde{c}\right)}{\partial x_j} + \frac{\partial \left(\overline{\rho u_j'' c''}\right)}{\partial x_j} = \frac{\partial}{\partial x_j}\left(\frac{\bar{\mu}}{\mathrm{Sc}}\frac{\partial \tilde{c}}{\partial x_j}\right) + \bar{\dot{\omega}}_c \qquad (4)$$

In the above equations ρ is the density, u_j is the velocity component in x_j direction, μ is the viscosity, Sc is the Schmidt number and $\dot{\omega}_c$ is the chemical reaction rate. An over-bar describes the application of the spatial filter while the tilde denotes Favre filtered quantities. The mean reaction rate can be modelled by either a simple Eddy-Break-Up (EBU) (Spalding, 1971) assumption which gives a reaction rate proportional to the time scale of turbulent mixing or by using more advanced models based on the flame surface density as described above. In the case of flame surface density approach, the mean reaction rate per unit volume is given by: $\dot{\omega}_c = R\Sigma$. Here R is a mean reaction per unit surface area and Σ is flame surface density, either modelled (Bray, 1990) or obtained by solving a full transport equation for the flame surface density (Prasad (1999) and Hawkes & Cant (2001)). Mean reaction rate per unit surface area R can be written as $\rho_u u_L$, where ρ_u is unburned mixture density and u_L is laminar flame velocity. The present analysis is carried to establish a level of

confidence on LES technique for explosions in confined chambers. Hence, we considered a simple algebraic expression for the flame surface density, deduced from the DNS analysis of thin premixed flames by Boger et al., (1998).

$$\Sigma = 4\beta \frac{\tilde{c}(1-\tilde{c})}{\overline{\Delta}} \tag{5}$$

where $\tilde{c}$ is Favre-filtered reaction progress variable, $\overline{\Delta}$ is the filter width and β is the model constant. In general the model constant β is known to depend on many physical parameters such as grid resolution, turbulence level and the chemistry. It can be considered as tuning parameter to obtain the desired result like in EBU models (Spalding, 1971). However for the present investigation, β is taken as 1.2 for all the simulations presented in this paper and this value has been achieved from the parametric analysis (Kirkpatrick et al. (2003) & Masri et al. (2006)) of propagating propane/air flames in similar type of explosion chambers. On the other hand β can be dynamically calculated to self-scale its value based on the wrinkling flame factor and the fractal dimension of the wrinkled flame front. Hence, one can expect that this procedure eventually predicts appropriate model coefficient even for large scale explosions, as it depends purely on the flame wrinkling characteristics. Such a model is under testing by the present authors. The above expression is similar to the Bray-Moss-Libby (BML) expression for flame surface density in RANS (Bray et al., 1989). The ratio $\overline{\Delta}/\beta$ represents the degree of sub-grid scale flame wrinkling.

4 Numerical procedure

The compressible version of the LES code PUFFIN (Kirkpatrick et al., 2003) originally developed by Kirkpatrick (2002) is used to simulate turbulent premixed

deflagrating flames propagating over solid obstructions mounted inside a laboratory scale combustion chamber. PUFFIN solves strongly coupled Favre-filtered mass, momentum, energy and reaction progress variable equations along with the state equation, which are written in boundary fitted coordinates and discretized by using the finite volume method. The discretization is based on control volume formulation on a staggered non-uniform Cartesian grid. A second order central difference approximation is used for diffusion, advection and pressure gradient terms in the momentum equations and for gradient in the pressure correction equation. Conservation equations for scalars use second order central difference scheme for diffusion terms. The third order upwind scheme of Leonard, QUICK (Leonard, 1979) and SHARP (Leonard, 1987) is used for advection terms of the scalar equations to avoid problems associated with oscillations in the solution. The QUICK scheme is also sometimes used for the momentum equations in areas of the domain where the grid is expanded and accurate calculation of the flow is less important. The equations are advanced in time using the fractional step method. Crank-Nicolson scheme is used for the time integration of momentum and scalar equations. A number of iterations are required at every time step due to strong coupling of equations with one other.

Solid boundary conditions are applied at the bottom, vertical walls, for baffles and obstacle by setting the normal and tangential velocity components to zero, which ideally represents impermeable and no-slip conditions. The walls and obstacles are isothermal and same temperature is maintained thorough out the simulations. The wall shear is calculated by the $1/7^{th}$ power-law wall function of Werner and Wengle (1991) taking the form of $\tau_w = W(\tilde{u}, y)$, where τ_w is the wall shear stress, W is a functional dependence, y is the distance of the grid point form the wall and $\tilde{u}$ is the tangential

velocity at y. Outflow boundary conditions are used at the open end of the combustion chamber. A non-reflecting boundary condition (Kirkpatrick, 2003), analogous to commonly used convective boundary condition, in incompressible LES is used to prevent reflection of pressure waves at this boundary. The initial conditions are quiescent with zero velocity and reaction progress variable. Ignition is modelled by setting the reaction progress variable to 0.5 with in the radius of 4 mm at the bottom centre of the chamber. This has produced reasonable agreement with experimental data. The impact of the radius of ignition sphere on the flame dynamics is not studied as it is beyond the scope of present work.

The equations, discretized as described above, are solved using a Bi-Conjugate Gradient solver with an MSI pre-conditioner for the momentum, scalar and pressure correction equations. The time step is limited to ensure the CFL number remains less than 0.5 with the extra condition that the upper limit for δt is 0.3ms. The solution for each time step requires around eight iterations to converge, with residuals for the momentum equations less than 2.5e-5 and scalar equations less than 2.0e-3. The mass conservation error is less than 5.0e-8. Simulations were carried in three dimensional non-uniform Cartesian co-ordinate system for compressible flow and having low Mach number. Since this type of flow involves large changes in density, high velocities and significant dilatation, all terms in the transport equations must be retained.

4.1 Computational domain

The computational domain has the dimensions of 50 x 50 x 250 mm (explosion chamber) where the explosion takes place and the flame propagates over the baffles and solid obstacle surrounded by solid wall boundary conditions. This domain is adequately extended to 325 mm in *x*, *y* and 250 mm in *z* direction with the far-field boundary conditions. In order to examine the solution dependence on grid resolution, three numerical grids have been employed. However in this paper we presented the results only for fine grid with 2.7 million grid points with 90 x 90 x 336 in x, y and z directions respectively.

5 Results and Discussions

LES results presented in this paper are for unsteady turbulent premixed deflagrating flames, ignited in an initially stagnant mixture of propane/air and propagating past built-in solid obstructions in an open end rectangular explosion chamber. Simulations were performed for 5 individual configurations shown in the Figure 2 and the details of the flame positions, flame speeds corresponding to the peak over pressure are presented in Table 1. The evolution of the turbulent flame is shown in terms of isotherms for configuration 1, 2 and 5 (from 500 to 2200 K) in Figure 3 at different instants after ignition. We choose only five instants which are relatively significant in the development of the propagating flame and the generation of overpressure inside the explosion chamber. All the configurations use a square solid obstruction running through the explosion chamber with the only difference in the number of baffles plates used. Configuration 1 uses three baffle plates (S1, S2 & S3), configuration 2 uses two baffle plates (S2 & S3) and configuration 5 uses only one baffle plate (S3) near the solid square obstruction. The time traces of over pressure, flame speed and

position for the three configurations with experimental measurements are shown in Figure 4 (a, b & c). For the same configurations flame speed and position are plotted against experimental measurements and shown in Figure 4 (d). This plot gives quantitative difference of flame speed in both the cases for any chosen flame front position.

As seen for configuration 1 shown in Figure 3(a), after the initialisation of the ignition, the leading edge of the flame starts expanding hemi-spherically (isotherm A) with velocity ΘS_L (Θ is the thermal expansion factor defined as density ratio of the fresh and burned fuel/air mixture) in axial direction and flame skirt elongates with laminar burning velocity, S_L in radial direction. The leading edge of the flame front propagates at the same speed i.e. ΘS_L until it reaches the first baffle plate. Once the flame hits the baffle plate, a rapid increase in flame speed followed by a sharp decrease is observed in Figure 4 (b) because of the local obstructions. After hitting the first baffle plate the laminar hemispherical structure of the flame is distorted and flame starts protruding through the narrow vents. As a result, the surface area of the flame brush increases, hence consuming more fuel/air mixture per unit time and propagating at relatively higher velocity through the un-burnt fuel/air mixture. As seen in isotherm B from Figure 3(a), this also results in wrapping and wrinkling of the flame around the local obstruction and around itself, which leads to the burnt gases trapping some un-burnt mixture on the obstruction's face. The trapped un-burnt gases will have significant contribution in increasing the over pressure at later stages (after third baffle plate). The flame front reaches the second plate at a progressive speed and creates pockets of fresh fuel/air mixture which eventually help to increase the over pressure at later stages of propagation. Surprisingly, this pocketing phenomenon is

only observed in case of configuration 1 and this is believed to be related to the high level of turbulence generated in the chamber. Eventually, the flame experiences wrinkling, stretching and a significant increase in surface area as it propagate further. At this stage, it can be noticed that the flame propagation speed increases rapidly and the flame front appears to be turbulent and more corrugated as it accelerates towards the third baffle. Increase in propagation speed due to the local turbulence causes further stretching and wrinkling of the flame. At this stage, the flame jets out of third baffle plate and encounters the solid square obstruction where the flame is further distorted and wrinkled, followed by an increase in surface area thereby boosting the reaction rate. Highly wrinkled flame starts wrapping around the solid square obstacle, which subsequently results in trapping of a high volume of un-burnt fuel/air mixture by flame at the up stream and the down stream of the square obstacle with in the recirculation zone. The highly wrinkled flame propagates past the obstacle and gets reconnected quickly with in the recirculation zone. The trapped gases will starts burning as the flame combines together and this has significant contribution in increasing the over pressure. The snapshots of the reaction rate at various instants after ignition from LES simulations are compared with the recorded high speed video images collected experimentally and shown in Figure 5 (a). The flame structure and the entrapment of the un-burnt gases are very well predicted at various stages by LES simulations.

Considering the configuration 2 with two baffle plates at location S2 and S3 along with a solid square obstruction as shown in 3 (b), a similar initial flame kernel propagating at a speed of ~4 m/s is observed like in configuration 1. As the flow encounters the baffle plate, laminar flame front get distorted by creating several

individual flamelets protruding through the narrow vents. Due to this distortion, the thin flame front wraps around the individual baffles by trapping certain amount of the un-burnt fuel/air mixture. The reaction rate increases due to the enhanced surface area which in turn suddenly accelerates and then decelerates the flame. Individual flame humps attempt to merge and propagate together as seen in the snapshots of the reaction rate in Figure 5 (b). With progressive flame speed (can be seen in Figure 4 (b & d)) flame encounters the second baffle plate, which leads to the generation of more turbulence. Due to the increase in the turbulence levels, flame is highly wrinkled and traps a huge amount of the un-burnt mixture up and down stream of the square obstacle. In order to identify the volume of the trapped un-burnt mixture streamlines are superimposed over reaction rate contours at various instants as shown in Figure 6 (b). All the streamlines originates at the ignition end of the chamber and tend to infinity in the fresh fuel/air mixture. It can be clearly seen that streamlines are deflected due to the local obstructions to form a trap and to push the fresh mixture. The amount of the mixture trapped is directly proportional to the strength of the turbulence and the number of the local obstructions used in the chamber.

For configuration 5 with only one baffle plate just upstream the square obstruction as shown in Figure 3 (c), propagating flame maintains laminar profile as shown in isotherm A, B and C corresponding to 6, 8 and 10.5 ms until it reaches baffle plate near the square obstacle. The flame surface area then increases due to the augmentation in flame curvature, which subsequently raises the consumption of the fuel/air mixture at any time in the reaction rate. As shown in Figure 4 (b & d) a gradual increase in the flame speed (~15m/s) is observed until the flame hits the baffle plate which increases the surface area due to the flame distortion. Similar tendency of

wrinkling as explained in case of configuration 1 can be observed as shown in Figure 3 (c) of isotherm D. Unlike in configuration 1, the variation in the flame speed is minor as the flame has enough time to interact with the baffle plate. Also it can be noticed from the snapshots of LES predictions and experimental images shown in 5(c), that the hemispherical structure of the flame started changing before hitting the baffle plate. Flame is less wrinkled in this situation and evidently can be seen from the isotherms D of 3 (a), (b) & (c). Distorted flame propagates further and encounters square obstacle which further distorts the flame. Distorted flame wrinkles the flame surface and generates vortices, which subsequently traps the un-burnt gases upstream and down stream of the square obstacle. It is noteworthy at this point that the volume of the trapped un-burnt fuel/air mixture is less than that of the configuration 1. This is because of the strength of the local turbulence encountered due to the flow conditions.

The peak over pressure for configuration 1 as shown in Figure 4 (a) from LES predictions is 110 mbar at 11.1 ms against the experimental measurements of 138 mbar at 10.3 ms. The peak overpressure in case of both LES and experiment occurs at a time where the flame from is reconnecting after having crossed over the square obstacle. At this point, burning of the trapped un-burnt gases down and upstream of the obstruction is also taking place. The time shift of the peak over pressure in case of the experiment could be because of uncertainties in establishing the time zero that marks ignition. However, there is no such problem with the LES predictions as ignition is initialized by setting reaction progress variable to 0.5 with in the radius of 4 mm. In configuration 2, the predicted peak over pressure from LES simulations is 96 mbar at 12.5 ms and this is roughly 13% less than the overpressure observed in configuration 1. From the experimental measurements, a peak overpressure of 119

mbar is observed at 12 ms. In case of configuration 5, the peak over pressure from the LES simulation is 64 mbar which is much less than for configuration 1 (approx. 41% lesser). This peak overpressure occurs at 14 ms which confirms that flame is travelling at lesser speed. Experimental measurements of peak overpressure for configuration 5 is 82 mbar occurring at 13.2 ms. The experimental peak pressure for configuration 5 is 41% less than for configuration 1 and occurs at a later time. In this case, the peak overpressure is occurring as the flame propagates furthest of the square obstacle and half way through to exit the chamber. This is just because the flame has travelled inside the chamber with laminar profile until it encounters the first baffle plate. A similar time shift in the incidence of the peak overpressure can be observed in this case and it is evident from the details of other configurations presented in Table 1, that the time shift is dependent on the condition of the individual experimental configuration. From these simulations it is evident that the magnitude of the over pressure generated in explosion chamber is dependent on the number and the position of solid obstructions with respect to the ignition point in combustion chamber.

Simulations of turbulent premixed flames by LES are qualitatively well predicted on par with the experimental measurements. These simulations substantiate the good representation of the flame position, speed, structure, interactions between flow and turbulence and reaction rate for various configurations. However, peak over pressure and its time of occurrence are predicted slightly less than that of experimental measurements. One possible reason for this discrepancy might be the sub-grid scale model employed to account the reaction rate. In case of thin premixed flames, chemical reaction takes place in thin propagating layers, referred as flamelets and this phenomenon is mostly in sub-grid scales. It is evident that the flame is thinner than

the grid resolution employed in the present simulation (Poinsot and Veynante, 2001). Employing a more complex combustion model (Gubba et al., 2007) may account for most of the sub-grid reaction rate. The second reason may be the laminar flame speed u_L is used in this model. Although instantaneous flame remains laminar with in these flamelets, the local flame speed can be affected by the flame stretch and curvature. Implementing the stretched laminar flame speed into the flame surface density model may produce better results. Further investigation in this direction are planned to be undertaken in order to assess the predictability of this model. Overall, LES simulations of premixed turbulent deflagrating flames by flame surface density model are very promising.

6 Conclusions

In the present work we have performed LES simulations of turbulent premixed deflagrating flames inside a novel explosion chamber, which can be rearranged into several configurations with the insertion or removal of baffle plates. Propane/air mixture at equivalence ratio 1.0 is ignited from stagnation. Five representative configurations were studied to understand the flame dynamics, flame-flow interactions and the related LES modelling issues. The key findings from the present study can be concluded as:

- In premixed explosions, the overpressure representing the generated energy in the chambers is directly proportional to the number and position of the baffles plates used in this study. The flame speed and the development of the reaction

zone are clearly dependent on the number of obstacle used and their blockage ratio.

- Extensive flame-flow interactions occur as the flame propagates past the baffle plate and the solid obstructions leading to higher burning rates. The flame progressively accelerates as it travels through the various stages of the chamber. Turbulent burning velocities of 12 to 14 m/s were achieved at the open end of the chamber. However there are no evidences to prove the presence of flame quenching due to elongation and stretching in the present study. This may be either due to the sub-grid scale model used for reaction rate or due to the volume of the chamber.
- Interestingly it is found that the trapped un-burnt gases are consumed later i.e. once the main flame leaves the chamber leading to subsequent oscillations in the pressure.

Overall, LES simulations substantiate the good representation of the flame position, speed, structure, interactions between flow and turbulence and reaction rate for various configurations.

References

Akkerman, V., Bychkov, V., Petchenko, A., and Eriksson, L. (2006) Flame oscillations in tubes with nonslip at the walls. *Combust. flame*, **145**, 675.

Aldredge, R.C., Vaezi, V., and Ronney, P. D. (1998). *Combust. flame*, **115**, 395.

Bauwens, C.R.L., Bauwens, L., and Wierzba, I. (2007) Accelerating flames in tubes-an analysis. *Proc. Combust. Instit.*, **31**, 2381.

Boger, M., Veynante, D., Boughanem, H., and Trouve, A. (1998) Direct numerical simulation analysis of flame surface density concept for large eddy simulation of turbulent premixed combustion. *Proc. Combust. Instit.*, **27**, 917.

Bradley, D., Cresswell, T.M., and Puttock, J.S. (2001) Flame acceleration due to flame-induced instabilities in large-scale explosions. *Combust. Flame,* **124**, 551.

Bradley, D. (2002) *Combust. Theory Modelling*, **6**, 361.

Bray, K.N.C., Champion, M., and Libby, P.A. (1989) Flames in stagnating turbulence in Turbulent Reacting Flows. *(Eds.) Borghi, R. and Murphy, S.N., Springer Publications:* New York, pp. 541-563.

Bray, K.N.C. (1990) Studies of turbulent burning velocity. *Proc. R. Soc. London*, Ser. A, **431**, 315.

Duwig, C., and Fuchs, L. (2007) Large eddy simulations of turbulent premixed combustion using marker field. *Combust. Sci. Tech.*, **179**:10, 2135-2152.

Fairweather, M., Ibrahim, S.S., Jaggers, H., and Walker, D.G. (1996) *Proc. Combust. Instit.*, **26**, 365.

Fairweather, M., Hargrave, G.K., Ibrahim, S.S., and Walker, D.G. (1999) *Combust. Flame*, **116**, 504.

Fureby, C., (2000) Large eddy simulation of combustion instabilities in a jet engine after burner model. *Combust. Sci. Tech.*, **161**:1, 213-243.

Fureby, C., (2005) *Proc. Combust. Instit.,* **30**, 593.

Germano, M., Piomeli, U., Moin, P., and Cabot, W.H. (1991) A dynamic subgrid–scale eddy viscosity model. *Phys. Fluids*, **A3** (7), 1760.

Gubba, S.R., Ibrahim, S.S., Malalasekera, W., and Masri, A.R. (2007) LES modelling of propagating turbulent premixed flames using a dynamic flame surface density model. *2nd ECCOMAS thematic conference on computational combustion*, *TU Delft, Delft, The Netherlands.*

Hawkes, E.R., and Cant, R.S., (2001) Implications of a flame surface density approach to large eddy simulation of premixed turbulent combustion. *Combust. Flame*, 126, 1617.

Hjertager, B.H., Fuhre, K., and Bjorkhaug, M. (1988) *Combust. Sci. Tech.,* **62**, 239.

Ibrahim, S.S., and Masri, A.R. (2001a) *J. Loss Prevention in the Process Industries*, **14**, 213.

Ibrahim, S.S., Hargrave, G.K., and Williams, C.T. (2001b) *Exp. Ther. Fluid Sci.*, **24**, 99.

Kang, Y., and Wen, J.X. (2004) Large eddy simulation of a small pool fire. *Combust. Sci. Tech.*, **176**:12, 2193-2223.

Kent, J.E., Masri, A.R., and Starner, S.H. (2005) A new chamber to study premixed flame propagation past repeated obstacles. *5th Asia-Pacific Conference on Combustion*, *The University of Adelaide, Adelaide, Australia*.

Kim, W., Menon, S., and Mongia, H. (1999) Large eddy simulation of a gas turbine combustor flow. *Combust. Sci. Tech.*, **143**, 25-63.

Kirkpatrick, M.P. (2002) A Large eddy simulation code for industrial and environmental flows. PhD Thesis, School of Aerospace Mechanical and Mechatronics eng. University of Sydney, Australia.

Kirkpatrick, M.P., Armfield, S.W., Masri, A.R., and Ibrahim, S.S. (2003) Large Eddy Simulation of a Propagating Turbulent Premixed Flame. *Flow Turb. Combust.*, **70,** 1.

Knikker, R., and Veynante, D. (2004) A dynamic flame surface density model for large eddy simulation of turbulent premixed combustion. *Phys. Fluids,* **16** (11), L91-L94.

Lee, T.W., and Lee, S.J. (2003) *Combust. Flame*, **132**, 492.

Leonard, B.P. (1979) A stable and accurate convective modelling procedure based on quadratic upstream interpolation. *Comp. Methods in Applied Mech. Eng.*

Leonard, B.P. (1987) Sharp simulation of discontinuities in highly convective steady flow. *NASA technical memorandum* 100240.

Lindstedt, R.P., and Sakthitharan, V. (1998) *Combust. Flame*, **114**, 469.

Makarov, D., Molkov, V., and Gostintsev, Yu. (2007) Comparision between RNG and fractal combustion models for LES of unconfined explosions. *Combust. Sci. Tech.*, **179**:1, 401-416.

Malalasekera, W., Dinesh, K.K.J. Ranga., Ibrahim, S.S., and Kirkpatrick, M.P. (2007) Large eddy simulation of isothermal turbulent swirling jets, *Combust. Sci. Tech.*, **179**:8, 1481-1525.

Masri, A.R., Ibrahim, S.S., Nezhat, N., and Green, A.R., (2000) *Exp. Ther. Fluid Sci.*, **21**, 109.

Masri, A.R., Ibrahim, S.S., and Cadwallader, B.J. (2006) Measurements and large eddy simulation of propagating premixed flames. *Exp. Ther. Fluid Sci.*, **30**, 687.

McMurthy, P.A., Menon, S., and Kerstein, A.R. (1993) Linear eddy modelling of turbulent combustion. *Energy and Fuels*, **7**, 817.

Moen, I.O., Knystautas, D.M., and Lee, J.M. (1980) *Combust. Flame*, **39**, 21.

Moen, I.O., Lee, H.S., Hjertager, B.H., Fuhre, K., and Eckhoff, R.K. (1982) *Combust. Flame*, **47**, 31.

Moin, P., Squires, K., Cabot, W., and Lee, S. (1991) A dynamic subgrid-scale model for compressible turbulence and scalar transport. *Phys. Fluids*, **A3**, 2746.

Molkov, V., Makarov, D., and Grigorash, A. (2004) Cellular structure of explosion flame: Modelling and large-eddy simulation. *Combust. Sci. Tech.*, **176**:5, 851-865.

Möller, S.I., Lundgren, E., and Fureby, C. (1996) Large eddy simulations of unsteady combustion. *Proc. Combust. Instit.*, **26**, 241.

Patel, S.N.D.H., Jarvis, S., Ibrahim, S.S., and Hargrave, G.W., (2002) *Proc. Combust. Instit.*, **29**, 1849.

Phylaktou, H., and Andrews, G.E. (1991) *Combust. Flame*, **85**, 363.

Prasad, R.O.S., and Gore, J.P. (1999) *Combust. Flame*, **116**, 1.

Pitsch, H., and Lageneste, D.D. (2002) Large–eddy simulation o f premixed turbulent combustion using a level-set approach. *Proc. Combus. Instit.*, **29**, 2001.

Poinsot, T., Veynante, D., and Candel, S. (1991) *J. Fluid Mech.* **228**, 561.

Poinsot, T., and Veynante, D. (2001) Theoretical and Numerical Combustion, R.T. Edwards, Philadelphia, USA.

Smagorinsky, J. (1963) General circulation experiments with the primitive equations, I, The basic experiment. *Monthly Whether Rev.*, **91**, 99.

Spalding, D.B. (1971) Mixing and chemical reaction in steady confined turbulent flames. *Proc. Combus. Instit.*, **13**, 649.

Starke, R., and Roth, P. (1989) *Combust. Flame,* **75**, 111.

Veynante, D., and Poinsot, T., (1997) Large eddy simulations of the combustion instabilities in turbulent premixed burners. Centre for Turbulence Research Annual Research Briefs, USA. pp. 253-275.

Werner, H. and Wengle, H. (1991) Large-eddy simulation of turbulent flow over and around a cube in a plate channel. *8th Symp. Turb. Shear Flows*, Munich, Germany.

Williams, F.A. (1985a) Combustion Theory, Benjamin, Menlo Park, CA.

Williams, F.A. (1985b) In the mathematics of combustion, (Ed.) Buckmasters, J. SIAM Philadelphia, pp. 97-131.

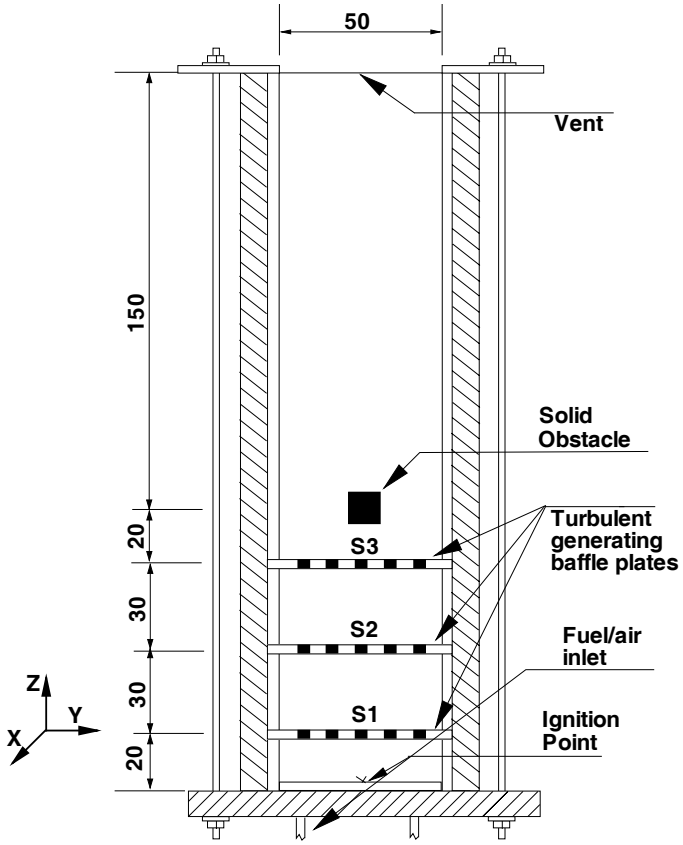

Figure 1 Schematic diagram of the premixed combustion chamber. All dimensions are in mm.

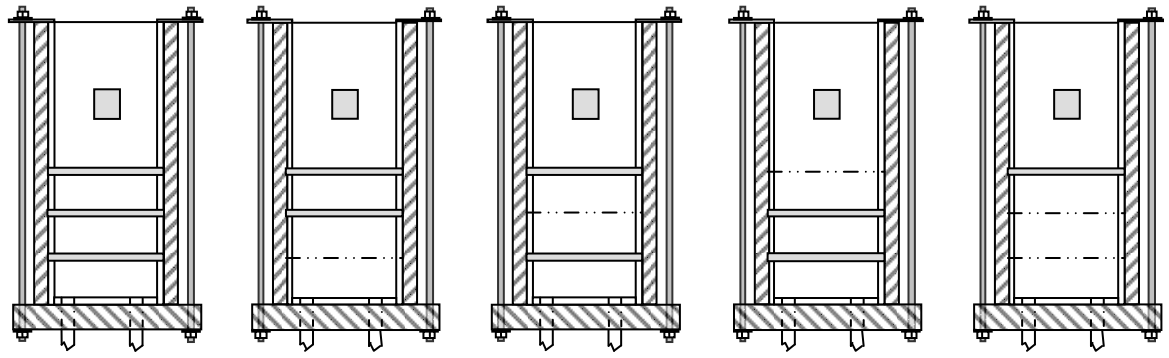

Configuration 1 Configuration 2 Configuration 3 Configuration 4 Configuration 5

Figure 2 Schematic diagrams of the various configurations used in the present simulations.

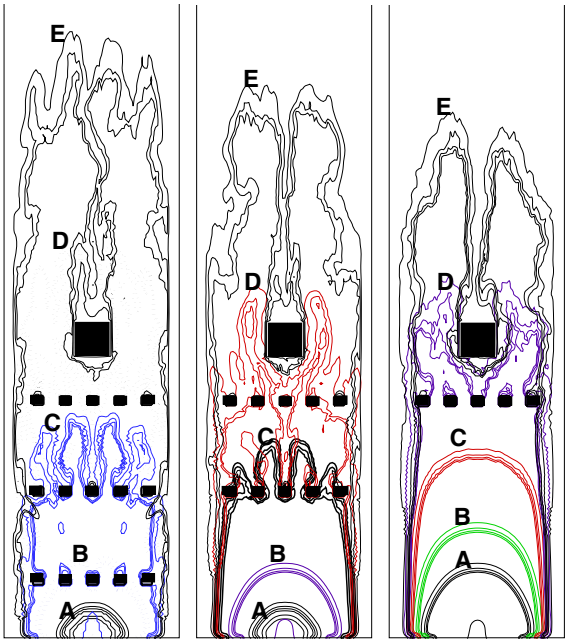

(a) (b) (c)

Figure 3 Development of the turbulent deflagrating flame in three different configurations are presented (a) Configuration 1; flame isotherms at 3.0, 6.0, 9.5, 10.5 and 11.3 ms corresponding to the positions A to E respectively. (b) Configuration 2; isotherms at 3.0, 6.0, 10.0, 11.5 and 12.5 ms corresponding to the positions A to E respectively. (c) Configuration 5; isotherms at 6.0, 8.0, 10.5, 13.0 and 14.0 ms corresponding to positions A to E respectively.

Table 1 Results from the LES simulations and experimental measurements are presented for various configurations.

Configuration	Turbulence generating grid				Experimental data sets				LES Predictions				Time shift
	S1	S2	S3	Sq. Ob.	Peak over pressure (mbar)	Time (ms)	Corresponding Flame position (m)	Corresponding Flame speed (m/s)	Peak over pressure (mbar)	Time (ms)	Corresponding Flame position (m)	Corresponding Flame speed (m/s)	LES - Exp
1	Y	Y	Y	Y	138.28	10.3	0.1	53.94	109.53	11.06	0.1785	81.83	0.74
2	-	Y	Y	Y	118.46	11.96	0.1	50.72	95.70	12.53	0.1815	76.582	0.57
3	Y	-	Y	Y	80.47	11.42	0.13	49.52	82.21	11.99	0.1805	80.728	0.57
4	Y	Y	-	Y	77.15	9.79	0.08	30.0	80.11	10.95	0.1555	64.92	1.16
5	-	-	Y	Y	82.03	13.25	0.176	75.2	63.82	13.97	0.1675	63.33	0.72

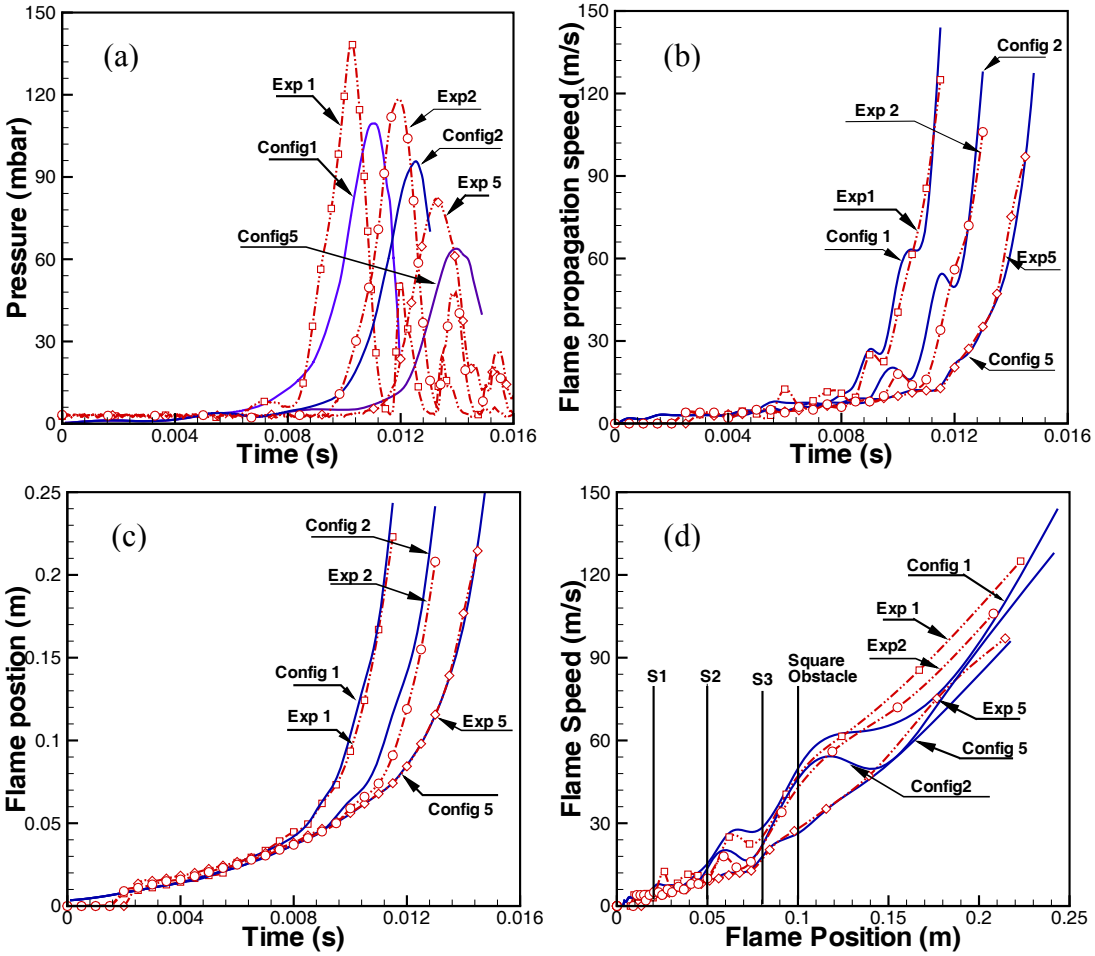

Figure 4 Time traces of LES simulations for three configurations (configuration 1, 2 and 5) with experimental measurements are presented. (a) Peak over pressure (b) Flame speed (c) Flame position (d) Flame speed is plotted against flame position.

Table 2 Percentage of pressure losses calculated and tabulated based on the over pressure of the configuration 1.

Configuration	Experimental		LES simulations		
	Over pressure (mbar)	% Pressure loss	Over pressure (mbar)	% Pressure loss	% Pressure loss based on individual experimental configuration
1	138.28	0.0	109.53	0.0	20.79
2	118.46	14.33	95.70	12.62	19.21
3	80.47	41.80	82.21	25.0	-2.16
4	77.15	44.20	80.11	26.86	-3.84
5	82.03	40.67	63.82	41.73	22.19

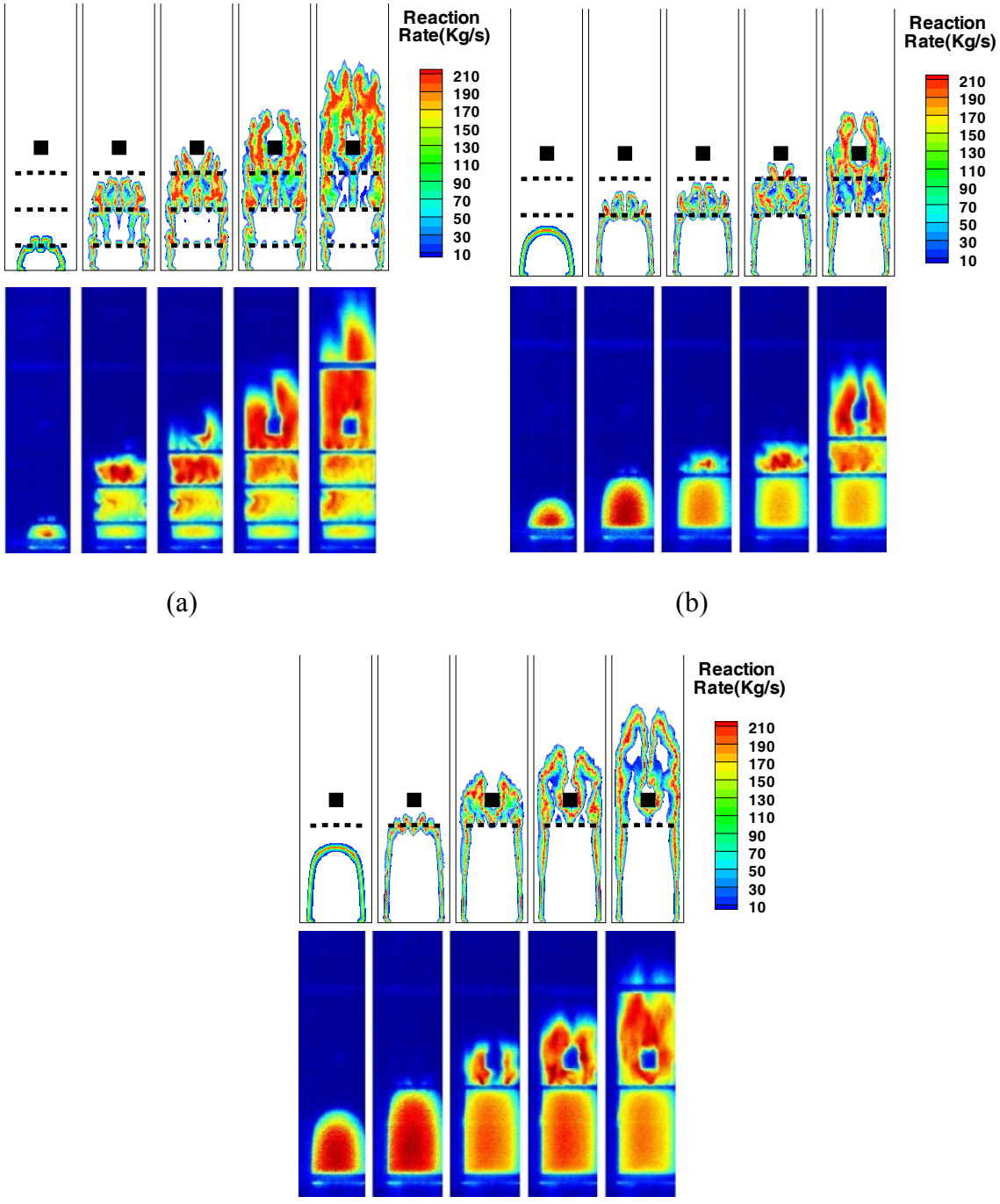

Figure 5 Sequence of images showing flame structure at different instants after ignition. Reaction rate contours generated from LES predictions are presented against high speed recorded video images of experiments. (a) Numerical snap shots for configuration 1 at 6, 9.5, 10.0, 10.5, and 10.8 ms are compared with experimental images at 6, 9.5, 10, 10.5 and 11.5 ms. (b) Numerical snap shots for configuration 2 at 8.0, 10.0, 11.0, 11.5 and 11.8 ms are compared with experimental images at 8.0, 10.0, 11.0, 11.5 and 12 ms.(c) Numerical snap shots for configuration 5 at 10.5, 12.0, 13.0, 13.5, and 14.0 ms are compared with experimental images at 10.5, 12.0, 13.0, 13.5, and 14.0 ms.

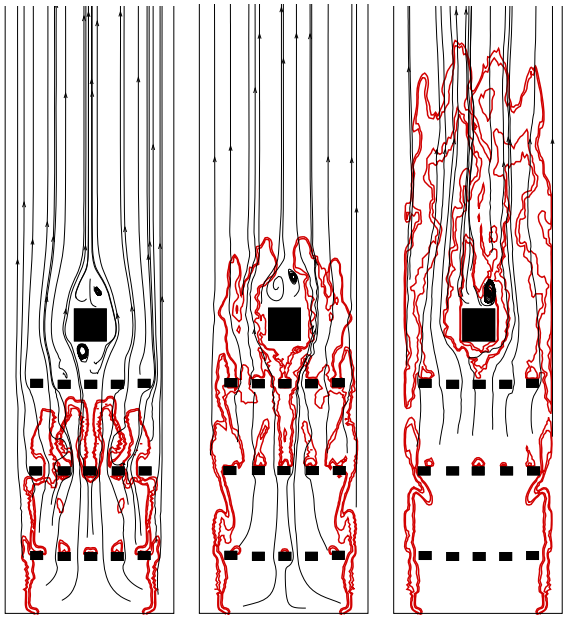

(a)

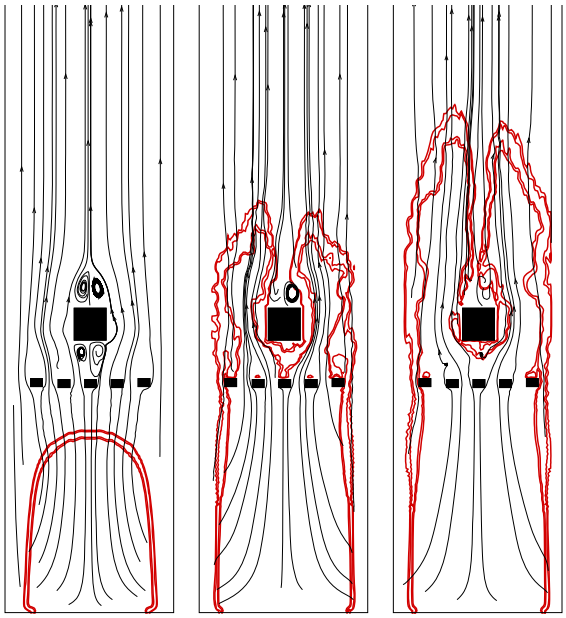

(b)

Figure 6 Streamlines are superimposed over reaction rate contour at various instants after ignition. (a) Configuration 1; at 9.5, 10.5, 11.3 ms. (b) Configuration 5; at 10.5, 13.0, 14.0 ms.